Conserved electron donor complex Dre2–Tah18 is required for ribonucleotide reductase metallocofactor assembly and DNA synthesis

Yan Zhang[a,1], Haoran Li[a,1], Caiguo Zhang[b,1], Xiuxiang An[b], Lili Liu[b], JoAnne Stubbe[a,c,2], and Mingxia Huang[b,2]

Departments of [a]Chemistry and [c]Biology, Massachusetts Institute of Technology, Cambridge, MA 02139; and [b]Department of Biochemistry and Molecular Genetics, University of Colorado School of Medicine, Aurora, CO 80045

Eukaryotic ribonucleotide reductases (RNRs) require a diferric-tyrosyl radical (Fe^{III}_2-Y•) cofactor to produce deoxynucleotides essential for DNA replication and repair. This metallocofactor is an important target of RNR-based therapeutics, although mechanisms of in vivo cofactor assembly, inactivation, and reactivation are poorly understood. Here, we demonstrate that the conserved Fe-S protein–diflavin reductase complex, Dre2–Tah18, plays a critical role in RNR cofactor biosynthesis. Depletion of Dre2 affects both RNR gene transcription and mRNA turnover through the activation of the DNA-damage checkpoint and the Aft1/Aft2-controlled iron regulon. Under conditions of comparable RNR protein levels, cells with diminishing Dre2 have significantly reduced ability to make deoxynucleotides. Furthermore, the kinetics and levels of in vivo reconstitution of the RNR cofactor are severely impaired in two conditional tah18 mutants. Together, these findings provide insight into RNR cofactor formation and reveal a shared mechanism underlying assembly of the Fe^{III}_2-Y• cofactor in RNR and the Fe-S clusters in cytosolic and nuclear proteins.

iron cofactor | iron regulon | dNTP pool | genome stability | S phase

Ribonucleotide reductase (RNR) converts NDPs to dNDPs by using radical-based chemistry and supplies the essential building blocks for DNA replication and repair (1–3). Class Ia RNR, conserved from bacteria to human, is composed of α and β subunits that form active quaternary structure(s) $(\alpha_2)_3(\beta_2)_m$ (m = 1 or 3) in eukaryotes (4–7). The α subunit contains the catalytic and allosteric sites that control overall activity and substrate specificity. The β subunit houses a di-iron center that generates and maintains a tyrosyl radical (Y•), which is essential to initiate nucleotide reduction in the catalytic site of the α subunit via a long-range radical transfer pathway (8, 9). In this study we focus on the mechanism by which the requisite diferric-tyrosyl radical (Fe^{III}_2-Y•) cofactor is generated in the β subunit of yeast RNR.

The *Saccharomyces cerevisiae* RNR holoenzyme is proposed to have an $(\alpha_2)_3\beta\beta'$ configuration, in which α, β, and β' are encoded by *RNR1*, *RNR2*, and *RNR4*, respectively. A fourth gene, *RNR3*, encodes an isoform of subunit α that normally is repressed and is inducible by genotoxic stress. The active form of yeast β_2 is a heterodimer (ββ') (10, 11). Only β is capable of iron binding and cofactor assembly, and consequently there is a maximum of one Y• per ββ'. However, β' is essential to maintain β in a conformation competent for iron binding both in vivo and in vitro (12–14).

Eukaryotic cells tightly control their RNR activity to maintain an adequately sized and balanced dNTP pool that ensures high-fidelity DNA synthesis. The levels and activities of *S. cerevisiae* RNR are regulated by both the cell cycle and environmental signals including genotoxic stress and low iron availability. Cells in S phase have increased expression of the α subunit and redistribution of ββ' from the nucleus to the cytoplasm, where the α subunit resides (15). In response to DNA damage, an activated Mec1–Rad53–Dun1 checkpoint kinase cascade increases RNR levels by phosphorylation-dependent removal of Crt1, the transcriptional repressor of *RNR2/3/4* (16). Checkpoint kinase-mediated phosphorylation also leads to degradation of two negative regulators of RNR: Sml1 that binds and inhibits subunit α (17, 18) and Dif1 that facilitates nuclear sequestration of ββ' (19, 20). Another negative regulator of RNR is the nuclear WD40 protein Wtm1, which binds and retains ββ' in the nucleus (21, 22). Under iron deficiency, mRNAs of *RNR2* and *RNR4* and, to a much greater extent, of *WTM1* are degraded in a *Cth1/Cth2*-dependent fashion as part of a metabolic remodeling process to conserve and optimize utilization of iron (23). Cth1/Cth2 belong to the iron regulon, a group of genes controlled by transcriptional factors Aft1 and Aft2 that are activated upon iron depletion (24).

An additional layer of RNR regulation, given that the level of Y• of the Fe^{III}_2-Y• cofactor is directly correlated with nucleotide reduction activity, involves the assembly and maintenance of this essential cluster. The cellular machinery required for these processes has been explored only recently (13, 25). The metallocofactor can be generated in vitro by self-assembly from apo-β_2, Fe^{II}, and O_2, with Fe^{II} supplying the required reducing equivalent (26, 27) (Eq. **1** and Fig. 1*A*). However, the self-assembly process is inefficient in general, pointing to the importance of a biosynthesis pathway for controlled cofactor assembly (28). The Y• in cells also can be destroyed rapidly by endogenous reductants or exogenous reducing agents such as hydroxyurea (HU) and triapine (29, 30, and thus must be repaired to restore RNR activity (Fig. 1*A*).

Significance

Ribonucleotide reductases (RNR) play a critical role in supplying cellular deoxynucleotide pools. Nucleotide reduction by class Ia RNR requires a diferric-tyrosyl radical cofactor, which is a target of anticancer agents. How this essential cofactor is assembled in vivo is not well understood. We show here that a conserved protein complex composed of the Fe-S–requiring Dre2 and the diflavin-requiring Tah18, previously shown to donate electrons for Fe-S cluster assembly for proteins found in the cytosol and nucleus, also is required for RNR cofactor assembly. Deficiency in this complex leads to activation of both the DNA-damage checkpoint and the iron regulon, linking iron homeostasis to maintenance of genome stability. These findings may provide new insights into development of RNR-targeted therapeutics.
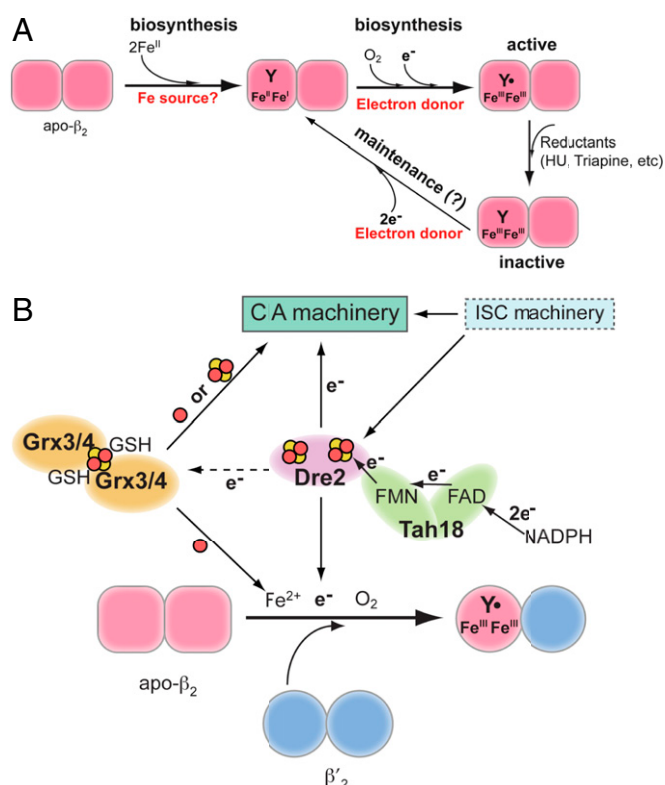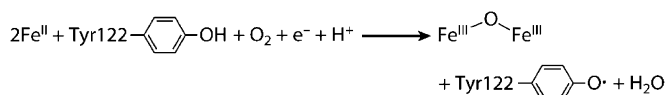
Fig. 1. The role of Dre2–Tah18 in RNR cofactor biosynthesis. (*A*) The proposed pathways for biosynthesis and maintenance of the Fe^{III}_2-Y• cofactor of class Ia RNR. The biosynthetic pathway requires delivery of two Fe^{II}/β and a reducing equivalent to carry out the four-electron reduction of O_2 to H_2O (Eq. 1); the other three electrons come from the two Fe^{II} and Tyr residue to form the Fe^{III}_2-Y•. The maintenance pathway may use the same source of reducing equivalents to convert the inactive Fe^{III}_2-Y cluster to Fe^{II}_2-Y, which subsequently forms Fe^{III}_2-Y• in the presence of O_2 via the biosynthesis pathway. (*B*) A model depicting the central role of the Dre2–Tah18 complex as a source of reducing equivalent for cluster assembly in RNR and cytosolic and nuclear Fe-S cluster-containing proteins. Assembly of Fe^{III}_2-Y• in β is facilitated by β', which stabilizes β in a conformation that allows iron binding. Grx3/4 functions in intracellular iron trafficking and is required for most iron-requiring pathways, including the biosynthesis of Fe-S clusters in the mitochondria (ISC) and cytosol (CIA) and Fe^{III}_2-Y• assembly in RNR (25). Electrons from NADPH are transferred via FAD and FMN, the two flavin cofactors in Tah18, to the Fe-S cluster(s) in Dre2, which subsequently deliver the electrons to proteins in the CIA pathway and β in RNR. Dre2–Tah18 also may provide reducing equivalents to facilitate iron release from the [2Fe2S]-GSH_2 cluster in the Grx3/Grx4 dimer.

$$2Fe^{II} + Tyr122-\!\!\!\bigcirc\!\!\!-OH + O_2 + e^- + H^+ \longrightarrow Fe^{III}\!\!\diagdown^{O}\!\!\diagup Fe^{III}$$
$$+ Tyr122-\!\!\!\bigcirc\!\!\!-O\cdot + H_2O$$

$$[1]$$

The key issues of in vivo RNR cofactor assembly are loading of Fe^{II} to apo-β_2 and delivery of the obligatory reducing equivalent (Eq. 1). In *S. cerevisiae*, two cytosolic monothiol glutaredoxins, Grx3 and Grx4, which form a dimer with a [2Fe2S]-GSH_2 cluster at the subunit interface, recently have been proposed to play an important role in the delivery of iron to Fe-S, heme, and di-iron–requiring proteins (25, 31, 32). Depletion of Grx3/4 in yeast cells reduced iron loading into $\beta\beta'$ and impaired the ability of RNR to make dNTPs; both effects are consistent with a role in providing iron to RNR (25).

Our previous study also led us to propose that the Fe-S cluster protein Dre2 is a conduit of the reducing equivalent required for RNR cluster assembly and for reduction of the Fe-S cluster in

Grx3/Grx4 for iron delivery (13) (Fig. 1*B*). This role was supported by a synthetic growth defect between *dre2* and *grx3/4* mutants and by the finding that depletion of Dre2 in yeast cells causes hypersensitivity to the Y•-quenching reagent HU and a decrease in both Y• content and RNR activity (13). However, these studies were complicated by the instability of $\beta\beta'$ in Dre2-deficient cells.

Recently Dre2 has been shown to form a complex with the diflavin reductase Tah18 (33, 34) and to supply reducing equivalents to the early steps of the cytosolic Fe-S assembly (CIA) pathway (33). Thus, it is possible that together Dre2–Tah18 donate the electron for RNR cluster assembly (Fig. 1*B*). This hypothesis is appealing, because we recently have shown that Fe^{III}_2-Y• maintenance of the *Escherichia coli* NrdB (β_2) is facilitated by a [2Fe-2S]-ferredoxin encoded by *yfaE*, which resides in the same operon as *nrdA* (α) and *nrdB* (β) (35). Although the *S. cerevisiae* ferredoxin-ferredoxin reductase (Fd-Fre) orthologs Yah1-Arh1 are localized exclusively in the mitochondria (36, 37), the Dre2–Tah18 pair has emerged as their cytoplasmic counterparts (33).

In this work, we have characterized the pleiotropic effects of Dre2–Tah18 deficiency on RNR including Cth1/2-mediated *RNR2*/*RNR4* mRNA degradation and activation of the DNA-damage checkpoint leading to RNR induction and activation. Furthermore, using genetic manipulations, we have developed methods of circumventing the variability of $\beta\beta'$ levels to determine the effect of Dre2–Tah18 deficiency on RNR cofactor assembly. We have found that the low $\beta\beta'$ levels in Dre2-depleted cells can be partially suppressed by an increase in intracellular manganese levels. Upon controlling for variability in $\beta\beta'$ levels, depletion of Dre2 causes a significant decrease in Y• content and RNR activity. Moreover, we took advantage of a *GalRNR4 Δcrt1* system in which β is constitutively overexpressed because of the removal of transcriptional repression and in which reconstitution of Y• and $\beta\beta'$ activity can be monitored over a time course upon induction of β' by turning on the *GAL* promoter. Under these conditions, we found that two *tah18* conditional mutants exhibit significant defects in both the kinetics and the maximum levels of Y• and $\beta\beta'$ activity reconstitution relative to the WT control. Together, our findings support the model that Dre2–Tah18 functions in RNR cluster assembly and raise the intriguing perspective that the same protein pair functions as a donor of reducing equivalents to two different types of cytosolic iron clusters: the Fe-S cluster in CIA and the di-iron cluster in RNR.

Results

GalDRE2 Mutant Has Lower Y• and β Levels Even in the Absence of the *RNR2/RNR4* Transcription Repressor Crt1. Because *DRE2* is essential for cell viability, the downstream effects of Dre2 deficiency can be investigated by replacing the native *DRE2* promoter with the glucose-repressible *GAL1* promoter to allow transcriptional shut-off. We have shown previously that Dre2 depletion in *GalDRE2* cells led to concurrent decreases in levels of Y•, $\beta\beta'$ activity, and $\beta\beta'$ proteins (13). To determine whether the decrease in $\beta\beta'$ protein levels is mediated transcriptionally or posttranscriptionally, we constructed a *Δcrt1GalDRE2* double mutant in which *CRT1*, the major transcriptional repressor of *RNR2* and *RNR4*, was removed. The protein levels of β and β' in *Δcrt1GalDRE2* cells were still threefold lower than in the *Δcrt1* single mutant, (Fig. 2*A*), suggesting that the decrease in $\beta\beta'$ levels in *GalDRE2* cells is mediated by a posttranscriptional mechanism. Moreover, the Y• content of *Δcrt1 GalDRE2* cells is 5.3-fold lower than that of *Δcrt1* (Fig. 2*B*). Thus, after correction for the difference in $\beta\beta'$ protein levels, Dre2 depletion in *Δcrt1* cells resulted in a twofold decrease in Y•/$\beta\beta'$ ratio.

The Decrease of ββ′ Levels in *GalDRE2* Mutant Is Mediated by *CTH2* and *CTH1*. A recently discovered mechanism of posttranscriptional regulation of *RNR2* and *RNR4* is targeted mRNA turnover mediated
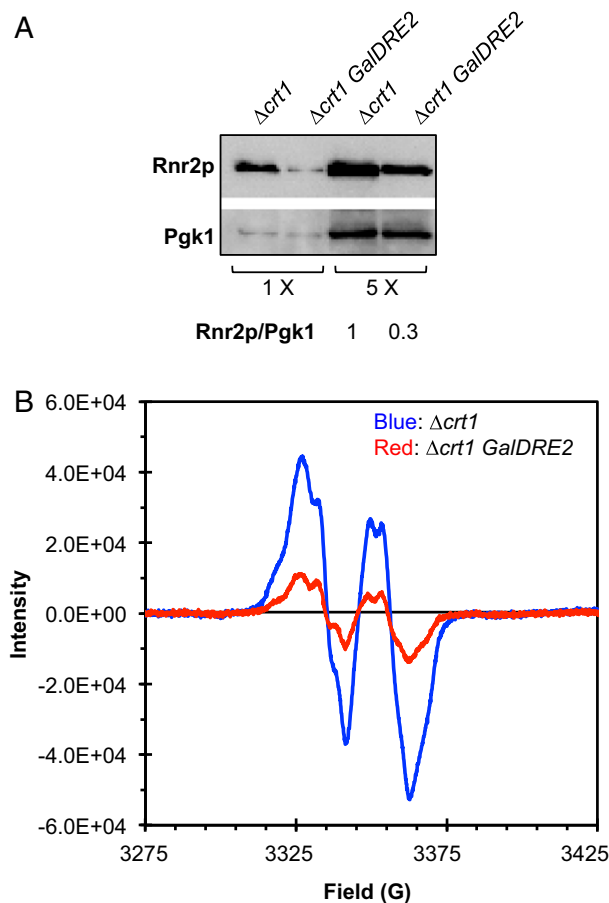
A

Fig. 2. The *GalDRE2* mutant has lower Y• and ββ′ levels even in the absence of the *RNR2/RNR4* transcription repressor Crt1. Cells from a galactose-containing plate (*GAL* on) were inoculated into glucose-containing liquid (*GAL* off) and grown at 30 °C for 24 h to reach log phase before being harvested for EPR and Western blotting. (*A*) Comparison of Rnr2 (β) levels in Δ*crt1* and Δ*crt1GalDRE2* cells by Western blot with Pgk1 as a loading control. Rnr2/Pgk1 ratios were quantified based on signal intensity. (*B*) Whole-cell EPR spectra of Δ*crt1* (blue, 8.4×10^9 cells/mL) and *GalDRE2* Δ*crt1* (red, 9.3×10^9 cells/mL).

by *Cth1* and *Cth2* (23), two homologous proteins that bind to specific AU-rich elements in the 3′ UTRs of many mRNAs including those of *RNR2* and *RNR4* (38). In response to iron deficiency, cells activate transcription of *CTH1* transiently and of *CTH2* persistently, which target specific mRNA degradation leading to metabolic reprogramming of iron utilization and iron storage (39, 40). To determine whether *CTH2* is induced in Dre2-depleted cells, we performed reverse transcription and quantitative real-time PCR (RT-qPCR) to compare *CTH2* mRNA levels in WT and *GalDRE2* mutant cells under *GAL* promoter-off conditions. *CTH2* mRNA is ~6.5-fold higher in *GalDRE2* cells than in WT cells (Fig. 3*A*). A similar increase in *CTH2* mRNA also was observed in Δ*crt1 GalDRE2* relative to Δ*crt1* cells, suggesting that induction of *CTH2* is caused by depletion of Dre2 instead of by removal of *CRT1*. Unlike *CTH2*, the mRNA level of *FET3*, another member of the iron regulon, is induced only slightly in *GalDRE2* (Fig. 3*A*).

Concurrent with an increase in *CTH2* levels, we observed a 2.5-fold decrease in *RNR2* and *RNR4* mRNA levels in *GalDRE2* cells (Fig. 3*B*). The decrease in *RNR2* and *RNR4* transcripts appeared to be mediated mainly by *CTH1/CTH2* because deletion of both genes in *GalDRE2* cells restores *RNR2* and *RNR4* mRNA levels to ~70% and 100% of those in WT cells (Fig. 3*B*). Interestingly, although Rnr4 (β′) protein in *GalDRE2* cells was

restored to close to WT levels by removal of *CTH1/CTH2*, no significant increase in Rnr2 (β) protein level was observed in Δ*cth1*Δ*cth2GalDRE2* cells relative to *GalDRE2* cells (Fig. 3*C*). The discrepancy between transcript and protein levels of *RNR2* likely reflects decreased stability of apo-β in Dre2-depleted cells.

Dre2 Depletion Activates both the DNA-Damage Checkpoint and Aft1/Aft2-Dependent *CTH2* Transcription and Thereby Exerts Complex Effects on RNR. We noted that induction of *CTH2* in Dre2-depleted cells is less robust (sixfold) than in the Δ*grx3*Δ*grx4* mutant (~10.5-fold), which activates transcription of many genes of the iron regulon including *FET3* (41) (Fig. 3*A*). *CTH2* transcription can be activated by both Aft1 and Aft2 (41, 42). Moreover, an endogenously tagged Cth2-GFP fusion protein has been shown to become more abundant in cells under HU-caused replicational stress (43), suggesting that *CTH2* expression may be subjected to other regulation in addition to Aft1/Aft2.

To determine whether the increased *CTH2* transcription in *GalDRE2* mutants is mediated by Aft1, Aft2, or the DNA replication checkpoint, we compared *CTH2* mRNA levels by RT-qPCR in WT cells, *GalDRE2* cells, and *GalDRE2* cells lacking *AFT1*, *AFT2*, or the checkpoint kinase *DUN1*. The *CTH2* mRNA level was unaffected in Δ*dun1* and was slightly lower in Δ*aft1* and Δ*aft2* cells (Fig. 4*A*). The increase of *CTH2* mRNA in the *GalDRE2* mutant was independent of *DUN1*, because the *CTH2* level in the Δ*dun1GalDRE2* mutant cells was comparable to that in *GalDRE2* cells. In contrast, *CTH2* mRNA levels decreased by 20% in the Δ*aft1GalDRE2* cells and 50% in Δ*aft2GalDRE2* double mutants relative to the *GalDRE2* single mutant (Fig. 4*A*). In keeping with the decrease of *CTH2*, *RNR2* mRNA was restored from 43% in the *GalDRE2* single mutant to ~80% in both Δ*aft1GalDRE2* and Δ*aft2GalDRE2* double mutants relative to the WT strain (Fig. 4*A*). Together, these data indicate that *Aft1/Aft2*-mediated induction of *CTH2* is responsible for the decrease of *RNR2* mRNA levels in the *GalDRE2* mutant.

We also observed an increase in *RNR3* mRNA levels in the *GalDRE2* mutant by RT-qPCR analysis. In contrast to *CTH2*, *RNR3* induction in *GalDRE2* cells was clearly *DUN1*-dependent and Aft1/Aft2-independent, because it was abolished in the Δ*dun1GalDRE2* but unchanged in Δ*aft1GalDRE2* and Δ*aft2GalDRE2* double mutants relative to the *GalDRE2* single mutant (Fig. 4*B*). Interestingly, *RNR3* also was moderately induced in Δ*aft1* and Δ*aft2* single mutants. Consistent with the increased *RNR3* mRNA levels, Rnr3 protein levels also were higher in *GalDRE2* and Δ*aft1* mutant cells than in the WT control (Fig. 4*C*). Induction of *RNR3* is a signature of activation of the Mec1–Rad53–Dun1 checkpoint kinase cascade (16, 44) (Fig. 4*D*). To determine further whether *GalDRE2* cells have a constitutively activated DNA-damage response, we monitored phosphorylation status of Dif1, the DNA-damage–regulated nuclear import facilitator of ββ′ that is phosphorylated in a *DUN1*-dependent manner in response to genotoxic stress (19, 20). A 3Myc-Dif1 from the *GalDRE2* and Δ*aft1* mutants exhibited a phosphorylation-specific slow mobility shift on SDS/PAGE, which is undetectable in the Δ*dun1GalDRE2* double mutant (Fig. 4*C*). Therefore, *GalDRE2*, Δ*aft1*, and, to a lesser degree, Δ*aft2* mutants all have a constitutively activated checkpoint. No further increase in *RNR3* levels or Dif1 slow mobility shift was seen in the Δ*aft1GalDRE2* and Δ*aft2GalDRE2* double mutants relative to the *GalDRE2* single mutant, suggesting that the signal leading to *RNR3* induction in *GalDRE2* and Δ*aft1*/Δ*aft2* is of the same nature, likely a perturbation in intracellular iron homeostasis (Fig. 4*D*).

Depletion of Dre2 Decreases ββ′ Activity. Considering the pleiotropic effects of Dre2 depletion on ββ′ function, including transcription, mRNA turnover, and subcellular localization (Fig. 4*D*), we directed our effort toward identifying conditions under which the ββ′ protein levels remain relatively unchanged before and after *GalDRE2* shut-off so that the effect on ββ′ activity can
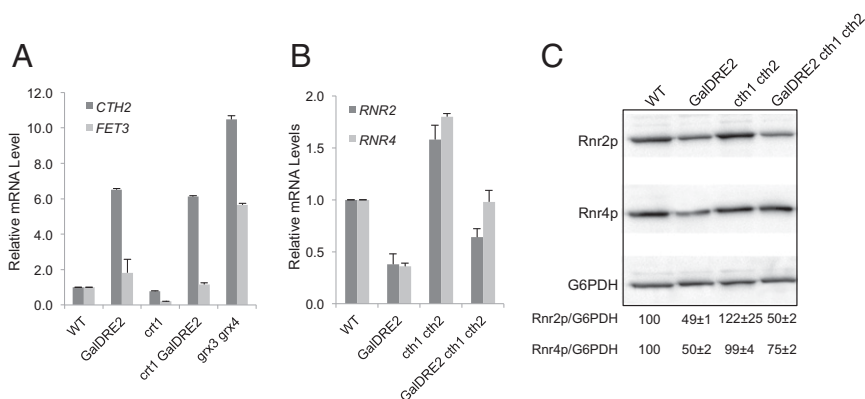
Fig. 3. The decrease in ββ′ levels in the *GalDRE2* mutant is mediated by *CTH1/CTH2*. (*A*) *CTH2* is induced in the *GalDRE2* mutant. Levels of *CTH2* and *FET3* mRNAs in WT, *GalDRE2*, Δ*crt1*, and Δ*crt1GalDRE2* cells were determined by reverse transcription and RT-qPCR. Signals of *CTH2* and *FET3* were normalized against that of *ACT1* in each strain, and the resulting ratios in WT cells were arbitrarily defined as onefold. Mutant Δ*grx3*Δ*grx4* was included as a positive control for iron regulon activation (41). (*B*) Comparison of *RNR2* and *RNR4* mRNA levels in WT, *GalDRE2*, Δ*cth1*Δ*cth2*, and *GalDRE2*Δ*cth1*Δ*cth2* cells by RT-qPCR as described in *A*. (*C*) Comparison of Rnr2 (β) and Rnr4 (β′) protein levels in WT, *GalDRE2*, Δ*cth1*Δ*cth2*, and *GalDRE2*Δ*cth1*Δ*cth2* cells by Western blot with G6PDH as a loading control. Rnr2/G6PDH ratios were quantified, and the average and SD from triplicates are shown.

be measured without concerns for drastically varying ββ′ levels. Manganese is known to be able to occupy the iron-binding site of class Ia RNR, resulting in catalytically inactive β₂ (45). A possible effect of increased cytosolic manganese levels is to form Mn-β that stabilizes the β protein. Because increasing intracellular manganese levels are known to down-regulate manganese uptake in WT cells (46), we chose the Δ*pmr1* mutant that is defective in manganese transport from the cytosol to Golgi (47) and that apparently is deficient in the negative feedback control of manganese uptake. As a result, Δ*pmr1* cells have ~10-fold elevated intracellular manganese levels (48, 49). To assess whether the increased intracellular manganese would affect β protein levels, we constructed the Δ*pmr1GalDRE2* double mutant. The β protein levels of the Δ*pmr1GalDRE2* cells remain comparable in *GAL*-repressed [yeast extract/peptone/dextrose (YPD)] and *GAL*-induced [yeast extract/peptone/Gal (YPG)] growth conditions (121% and 180%, respectively) but in *GalDRE2* single mutant varied by threefold in the YPD (47%) and the YPG (130%) conditions (Fig. 5*A*). The changes in β protein levels were mirrored in changes in *RNR2* mRNA levels. Consistent with the notion that *CTH2* induction leads to *RNR2* mRNA degradation, we found that the levels of *CTH2* transcript in Δ*pmr1GalDRE2* double mutant were much lower than those in *GalDRE2* single mutant under *GAL*-repressed (YPD) conditions (Fig. 5*B*).

Taking advantage of the comparable protein levels of β and β′ in the Δ*pmr1GalDRE2* cells in the *GAL*-repressed and *GAL*-induced states (Fig. 5*A*), we measured and compared the ββ′ activity of Δ*pmr1GalDRE2* cells grown in YPD and YPG by a permeabilized cell-based RNR activity assay (13). The activity of ββ′ in Δ*pmr1GalDRE2* cells is 6.5-fold lower under Dre2-repressed (YPD) conditions than in Dre2-induced (YPG) conditions (Fig. 5*C*, open circles versus filled circles). Under *GAL*-induced conditions, the ββ′ activity of Δ*pmr1GalDRE2* cells is ~40% higher than in *GalDRE2* cells (Fig. 5*C*, filled circles versus filled triangles), as is consistent with ~40% higher protein levels of β (Fig. 5*A*, lanes 3 and 5). Under Dre2-repressed conditions the ββ′ activity of Δ*pmr1GalDRE2* cells is as low as that of *GalDRE2* cells (Fig. 5*C*, open circles and open triangles), although Δ*pmr1GalDRE2* has 2.5-fold more of ββ′ protein (Fig. 5*A*, lanes 1 and 3). Collectively, these results indicate that Dre2 is required for the formation of catalytically active ββ′.

The proposal that Dre2 serves as the electron donor for cluster assembly in β requires a transient interaction between them. We thus performed reciprocal immunoprecipitation experiments in the strains containing either N-terminally epitope-tagged [3xMyc]*DRE2*

or [3xMyc]*RNR2* under their respective native promoters. The anti-Myc immunocomplex from [3xMyc]*DRE2* cells brings down not only [3xMyc]Dre2 but also Rnr2 (Fig. 5*D*, lanes 2 and 6, respectively). Conversely, we detected both [3xMyc]Rnr2 and Dre2 in the anti-Myc immunocomplex from [3xMyc]*RNR2* cells (Fig. 5*D*, lanes 8 and 4, respectively). Together, these results indicate that Dre2 and β can exist in the same protein complex in vivo, as is consistent with the model that Dre2 is involved in delivering the reducing equivalent to β for its cofactor assembly.

Conditional Mutants of *tah18* Exhibit Slow S-Phase Progression and Synthetic Growth Defect with *GalRNR4*. The diflavin reductase Tah18 forms a stable complex with Dre2 to transfer electrons from NADPH to Dre2's Fe-S clusters. We inferred that inactivation of Tah18 would have effects on RNR similar to that of Dre2 depletion. *TAH18* is essential for viability. A previous study has identified two temperature-sensitive (ts) mutant alleles of *TAH18*, *tah18-5H8*, and *tah18-5I5* (34). We characterized the original *tah18* ts strains on HU-containing plates and found that *tah18-5I5* was hypersensitive to HU at the permissive temperature 25 °C (Fig. S1). Moreover, both *tah18* ts mutants exhibited defects in cell-cycle progression upon release from α factor-mediated G1 arrest: a prolonged S phase for *tah18-5I5* and a delay at the G1/S boundary for *tah18-5H8* (Fig. S2).

HU sensitivity and defects in G1/S transition or S-phase progression are characteristics of mutants deficient in DNA replication or cellular dNTP pools. To investigate whether the RNR cluster formation is defective in the *tah18* ts mutants, we used whole-cell EPR to measure and compare Y• contents in the mutants and their isogenic WT strain. The EPR spectra of these strains had a very high background (Fig. S3) relative to the W303 and S288C strains (11, 13) and thus impeded accurate quantitation. To circumvent this problem, we moved the two *tah18* ts mutant alleles into the W303 strain background by crossings with a W303 WT parental strain six times. The outcrossed mutants retained the *ts* and cell-cycle delay phenotypes but no longer showed obvious HU sensitivity, suggesting that background mutations in the original strains contribute to the growth defect on HU. Interestingly, both the *tah18-5I5* and *tah18-5H8* mutants showed a delay in S-phase progression after being released from G1 (Fig. 6*A*). Moreover, both *tah18-5I5* and *tah18-5H8* enhance HU sensitivity of the *GalRNR4* mutant in which the chromosomal *RNR4* promoter was replaced by the glucose-repressible *GAL1* promoter, on a glucose-containing plate (Fig. 6*B*), suggesting exacerbation of RNR deficiency when both Rnr4 (β′) and Tah18 are compro-
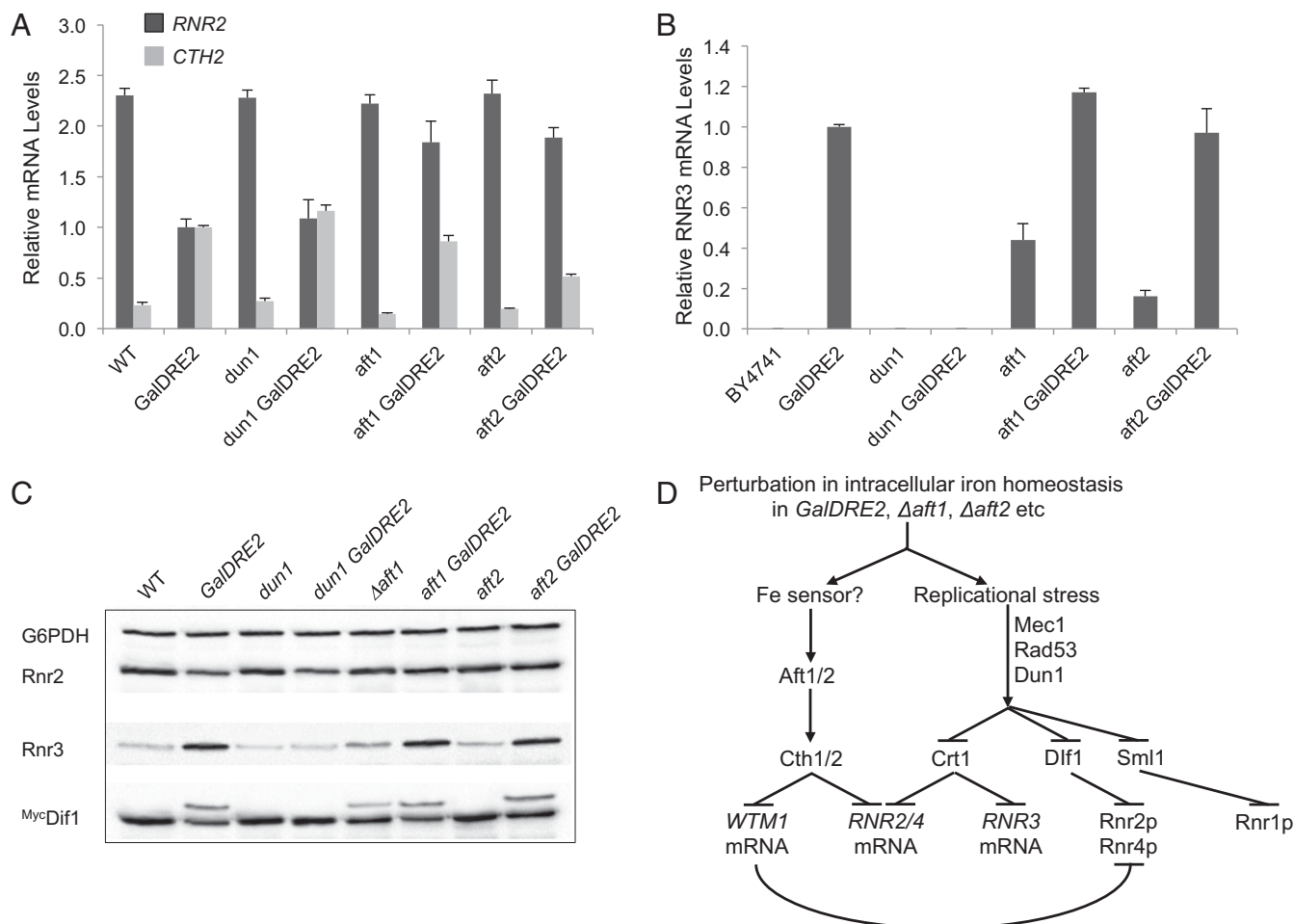
Fig. 4. The *GalDRE2* mutant exhibits checkpoint activation. (*A*) Comparison by RT-qPCR of *RNR2* and *CTH2* mRNA levels in WT, *GalDRE2* single mutants, and *GalDRE2* double mutants with Δ*dun1*, Δ*aft1*, and Δ*aft2* as described in Fig. 3*A*. The *RNR2/ACT1* and *CTH2/ACT1* ratios of *GalDRE2* were arbitrarily defined as onefold. (*B*) Checkpoint-dependent *RNR3* induction in the *GalDRE2* mutant. *RNR3* mRNA levels were determined in WT and mutant cells grown in YPD (*GAL* off) by RT-qPCR, with the *RNR3/ACT1* ratio of *GalDRE2* defined as onefold. (*C*) Checkpoint-mediated phosphorylation of Myc3-Dif1 in the *GalDRE2* mutant, manifested as the slower mobility band on Western blot (20). (*D*) A scheme depicting the downstream events in cells deficient in Dre2 or Aft1/2. Cth2 is induced in Dre2-depleted cells via Aft1/Aft2 activation, leading to degradation of *RNR2/RNR4* mRNAs and, to a much greater extent, of the mRNA of *WTM1*, which encodes a nuclear anchoring protein of Rnr2/4 (21, 22). Moreover, the DNA-damage checkpoint is activated in cells lacking Dre2 or Aft1/Aft2, causing phosphorylation-dependent removal of three negative regulators of RNR: Crt1 that represses transcription of *RNR2/3/4*, Sml1 that inhibits Rnr1 (α), and Dif1 that imports Rnr2/4 (ββ′) into the nucleus away from α.

mised. The synthetic growth defect between *GalRNR4* and *tah18* ts mutants is reminiscent of the synthetic defect observed between Δ*rnr4* and *GalDRE2* (13).

Concurrent Decreases in ββ′ Activity and Proteins Levels in the *tah18* ts Mutants. As anticipated, the outcrossed *tah18* ts mutants have a much cleaner EPR background and thus allow quantitative comparison of the Y• content in WT and mutants. Both *tah18-5I5* and *tah18-5H8* mutants have ~50% of Y• content seen in the WT strain even at the permissive temperature 25 °C (Fig. 6*C*). Consistent with the low Y• levels, the activities of ββ′ of the two *tah18* ts mutant cells were ~40% of activities of the WT cells when normalized by cell numbers (Fig. 6*D*). However, when probing for β protein, we found that the two *tah18* ts mutants also had a much lower β levels (Fig. 6*E*). The protein levels of β in the *tah18-5H8* mutant exhibited a further and dramatic decline when the cells were shifted from 25 °C to the nonpermissive temperature 37 °C, dropping to ~20% of the WT levels after 2 h at 37 °C and becoming undetectable after 4 h (Fig. 6*F*). Consistent with the decrease in β protein levels, RNR activity of *tah18-5H8* dropped to 10% of the WT levels 3 h after being shifted to 37 °C (Fig. 6*G*).

Thus, as in Dre2-depleted cells, the concurrent decrease in protein levels and activity of ββ′ complicated the assessment of the effect of inactivating Tah18 on RNR.

Inactivation of Tah18 at Nonpermissive Temperature Impairs Formation of Y• and Reconstitution of ββ′ Activity upon Induction of β′ in *GalRNR4* Cells. To circumvent the effect of Tah18 inactivation on β protein stability, we searched for conditions under which the β protein level is constant and not rate-limiting for measurement of Y• content and ββ′ activity. We have shown previously that induction of β′ in *GalRNR4* cells leads to rapid and efficient Fe^{III}_2-Y• formation up to fourfold of the level in WT cells (13). *GalRNR4* cells under *GAL*-repressed conditions accumulate five- to 10-fold more β protein than WT cells because activation of the Mec1-Rad53-Dun1 checkpoint leads to the removal of the transcriptional repressor Crt1. Upon induction of β′, formation of the active ββ′ and replenishment of cellular dNTP pools gradually diminishes the checkpoint signaling, and the levels of both β and Y• eventually return to those of WT cells because of Crt1-mediated negative feedback regulation (13, 16).
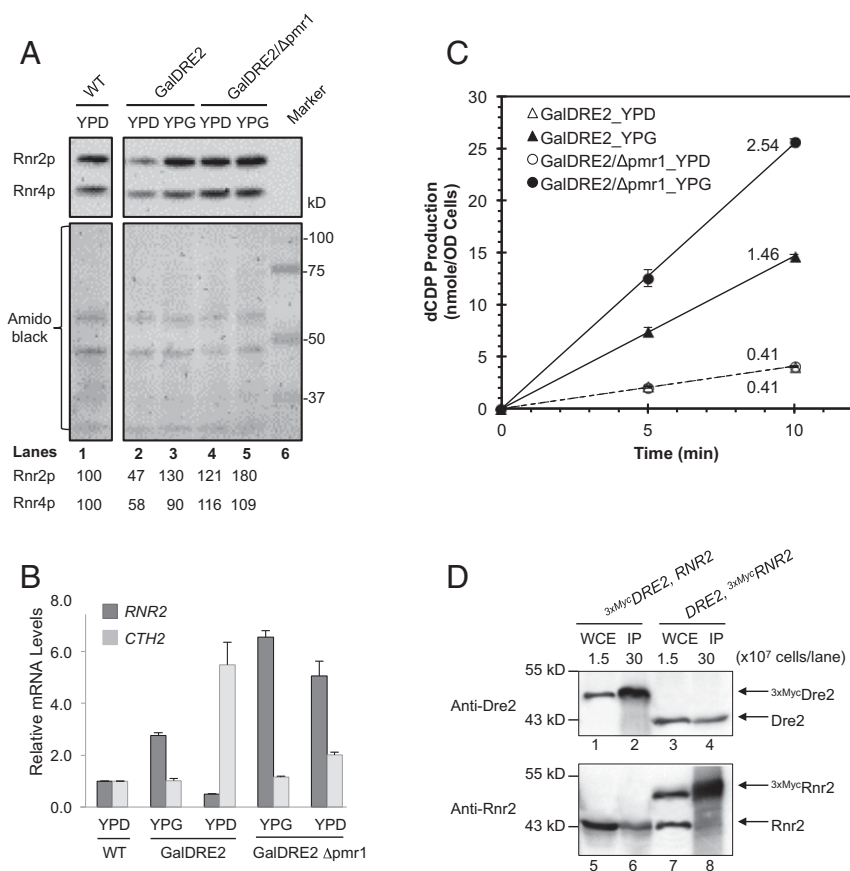
Fig. 5. Depletion of Dre2 causes decrease in ββ′ activity. (*A*) Comparison of Rnr2 protein levels in *GalDRE2 Δpmr1* and *GalDRE2* cells under *GAL*-on (YPG) and *GAL*-off (YPD) conditions. Total protein extract from an equal number of cells was loaded for each sample. The protein blot was probed with anti-Rnr2 and anti-Rnr4 (*Upper*) and stained with amino black (*Lower*) as a control for loading. Relative Rnr2 and Rnr4 signals are shown. (*B*) Removal of *PMR1* in *GalDRE2* cells abolished induction of *CTH2* and decrease of *RNR2* under *GAL*-off conditions. Relative levels of *RNR2* and *CTH2* mRNAs were determined by RT-qPCR and normalized against *ACT1* mRNA signals; the resulting ratios in WT cells were arbitrarily defined as onefold. (*C*) Comparison of ββ′ activities of *GalDRE2 Δpmr1* and *GalDER2* cells under *GAL*-on (YPG) and *GAL*-off (YPD) conditions. The ββ′ activity of each sample was assayed in permeabilized cells in the presence of an excess of α as previously described (13). The ββ′ activities for GalDRE2_YPD, GalDRE2_YPG, GalDRE2/Δpmr1_YPD, and GalDRE2/Δpmr1_YPG are 0.41, 1.46, 0.41, and 2.54 nmol dCDP/min in OD_{600} cells, respectively. (*D*) Coimmunoprecipitation of Dre2 and Rnr2 (β). Whole-cell extracts (WCE) of the [3Myc]*DRE2* (AXY1767) and [3Myc]*RNR2* (MHY340) strains were incubated a with anti-Myc monoclonal antibody 9E10. The immunoprecipitates (IP) were brought down with Protein A beads, and the protein blots were probed with polyclonal anti-Dre2 (lanes 1–4) and anti-Rnr2 (lanes 5–8) antibodies. The WCE lanes were loaded with lysates of 1.5×10^7 cells, and the IP lanes contained immunoprecipitates from lysates of 3×10^8 cells.

We capitalized on the inducible *GalRNR4* system and the conditional *tah18* ts mutant alleles to investigate whether Tah18 is required for the Y• cofactor formation upon β′ induction by generating *GalRNR4 tah18* double mutants. To remove Crt1-mediated negative feedback, we deleted *CRT1* in *GalRNR4 TAH18* (expressing WT Tah18) and *GalRNR4 tah18*-ts strains so that β is constitutively overexpressed and consequently is not rate-limiting for reconstitution of Y• and ββ′ activity upon induction of β′. Both *tah18-5H8* and *tah18-5I5* mutants exhibited lower Tah18 protein levels that dwindled quickly when shifted to the nonpermissive temperature 30 °C (Fig. S4). As expected, induction of β′ at 30 °C in the *GalRNR4 Δcrt1 TAH18* cells led to a time-dependent increase of Y• signal, reaching a plateau that was approximately fourfold higher than that of a WT W303 strain (Fig. 7 *A*, *B*, and *E*). In contrast, formation of Y• signal in *GalRNR4 Δcrt1 tah18-5H8* cells (Fig. 7*C*) and *GalRNR4 Δcrt1 tah18-5I5* cells (Fig. 7*D*) upon β′ induction at 30 °C occurred at a much slower pace and reached a plateau that was only 25% of the level in *GalRNR4 Δcrt1 TAH18* cells (Fig. 7*E*).

The β protein of the *GalRNR4 Δcrt1 TAH18*, *GalRNR4 Δcrt1 tah18-5H8*, and *GalRNR4 Δcrt1 tah18-5I5* cells remained at a constitutive level that is much higher relative to the W303 WT strain over the time course of the experiments as a result of loss of Crt1-mediated transcriptional repression (Fig. 7*F*). Under such conditions, induced expression of β′ protein becomes the rate-limiting step in ββ′ formation and cluster assembly so that the level of Y• formation would be proportional to the level of β′ protein induced. The time course and levels of induced β′ protein were comparable in *GalRNR4 Δcrt1 TAH18* cells and *GalRNR4 Δcrt1 tah18-5H8* cells. In both strains, β′ levels became detectable at 2 h and plateaued at 5 h (Fig. 7*E*), as was consistent with the time course of Y• appearance and increase that reached a plateau at 5 h (Fig. 7*E*). On the other hand, β′ induction and Y• formation in *GalRNR4 Δcrt1 tah18-5I5* cells occurred at a slower pace, becoming detectable at 3 h and reaching a plateau at 6 h (Fig. 7 *E* and *F*). Nevertheless, upon reaching the plateau (6 h for *GalRNR4 Δcrt1 TAH18* and *GalRNR4 Δcrt1 tah18-5H8* cells and 8 h for *GalRNR4 Δcrt1 tah18-5I5* cells), the levels of β and β′ proteins were comparable in all three strains, but the Y• levels of *GalRNR4 Δcrt1 tah18-5H8* cells and *GalRNR4 Δcrt1 tah18-5I5* cells were only ~25% of that of *GalRNR4 Δcrt1 TAH18* cells. As we have shown previously (13), there is a good correlation between the Y• signal determined by EPR and the ββ′ activity measured by the permeabilized cell-based RNR activity
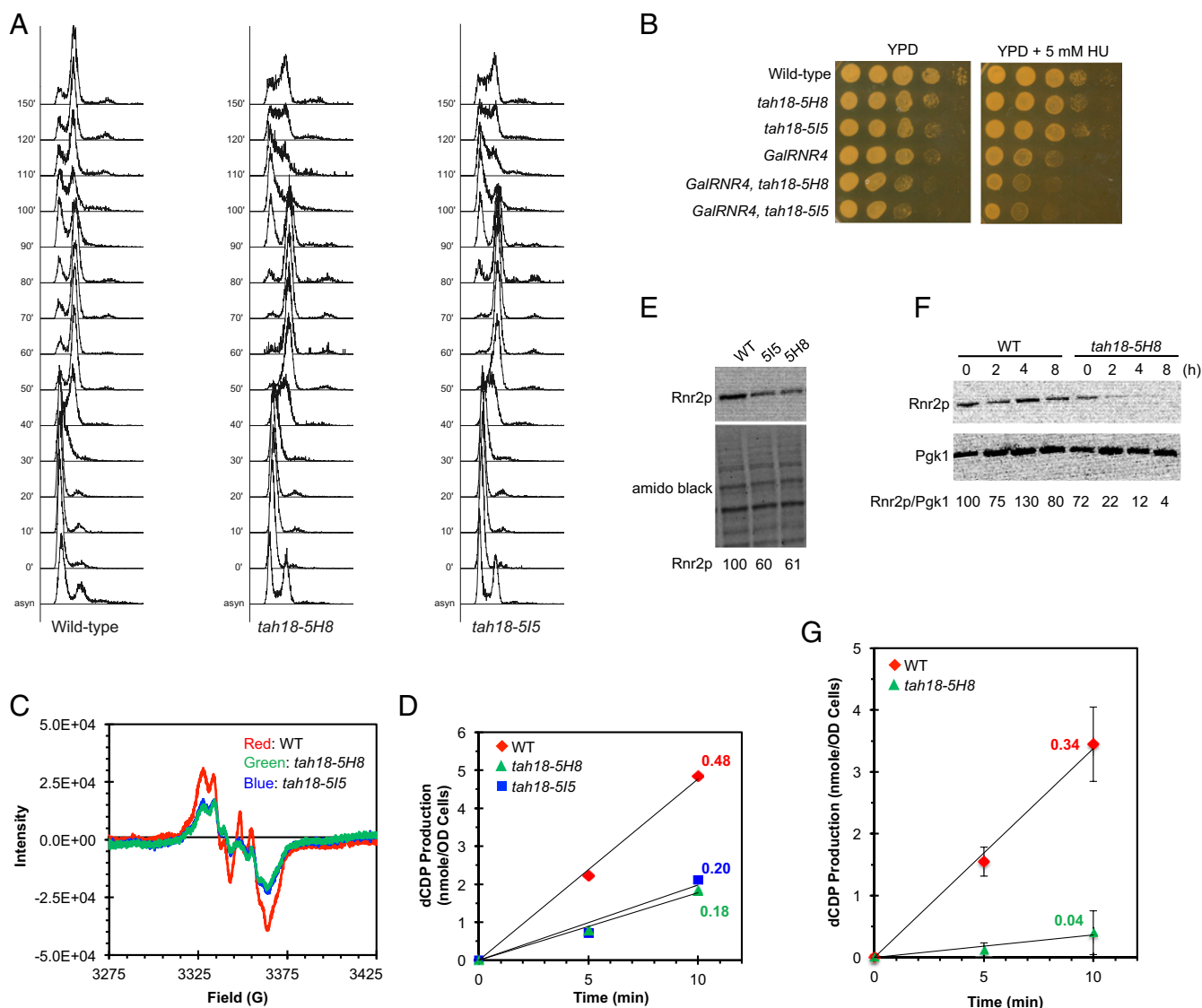
Fig. 6. The *tah18* ts mutants exhibit S-phase defects and a concurrent decrease in Y• content and β protein levels. (*A*) The defect in S-phase progression of *tah18* ts mutants. WT and *tah18* mutant cells from log-phase cultures were synchronized in G1 at 25 °C before being shifted to 37 °C for 1 h and released into the cell cycle at 37 °C. Cells were taken at the indicated time points for analysis of DNA content by flow cytometry. (*B*) Synthetic growth defect in *tah18* ts mutants and *GalRNR4*. Both the WT and *tah18* ts mutant strains were grown in galactose-containing medium (*GAL*-on) to log phase at 23 °C. Tenfold serial dilutions of each culture, starting at 10⁶ cells, were dot-plated on glucose-containing plates (YPD, *GAL* off) or YPD containing 5 mM HU and were incubated at 23 °C for 2.5 d before being imaged. (*C*) Measurement of Y• in WT, *tah18-5H8*, and *tah18*-5I5 mutants by whole-cell EPR analysis. Cells from log-phase culture at 25 °C were washed in ice-cold PBS, resuspended in PBS with 30% glycerol at a density of ~6.5 × 10⁹ cells/mL, and packed into EPR tubes. (*D*) Measurement of ββ′ activity by CDP reduction in permeabilized cells of WT, *tah18-5H8*, and *tah18-5I5* mutant strains in the presence of an excess of α. The ββ′ activities for WT, *tah18-5H8*, and *tah18-5I5* are 0.48, 0.18, and 0.20 nmol dCDP/min in OD₆₀₀ cells, respectively. (*E*) Comparison of Rnr2 protein levels in WT, *tah18-5H8*, and *tah18-5I5* mutant cells grown at 25 °C. The protein blot was probed with anti-Rnr2 and stained with amido black as a control for loading. Relative Rnr2 signals were quantified. (*F*) Comparison of Rnr2 protein levels in WT and *tah18-5H8* cells at 37 °C. Cells were grown to log phase at 25 °C, shifted to 37 °C at time 0, and harvested at the indicated time points for protein extraction and Western blotting. (*G*) Measurement of ββ′ activities by CDP reduction in permeabilized WT and *tah18-5H8* cells 3 h after cells were shifted to 37 °C, in the presence of an excess of α. The ββ′ activities for WT and *tah18-5H8* are 0.34 and 0.04 nmol dCDP/min in·OD₆₀₀ cells, respectively.

assay in these strains (e.g., ββ′ activities at 2 h after β′ induction are shown in Fig. S5). Thus these findings strongly support our model that Tah18 is required for de novo formation of the Fe^{III}_2-Y• cofactor in ββ′.

Discussion

In this work, we demonstrated that Dre2–Tah18, a protein complex recently identified as a donor of reducing equivalents to the CIA machinery (33), also plays a critical role in formation of the Fe^{III}_2-Y• cofactor in RNR. Our efforts to determine the con-

tribution of Dre2–Tah18 to RNR function were complicated by the decrease in ββ′ levels in *dre2* and *tah18* mutant cells. Our studies to understand the molecular basis for the decrease in ββ′ associated with Dre2–Tah18 inactivation thus have unexpectedly unveiled important regulatory mechanisms linking RNR stability with iron limitation and activation of the DNA-damage checkpoint.

First, we found that depletion of Dre2 induces *CTH2* transcription in an Aft1/Aft2-dependent manner. Previous studies have suggested that Aft1/2 sense cellular iron levels by responding to deficiency in the mitochondrial iron-sulfur cluster (ISC) as-
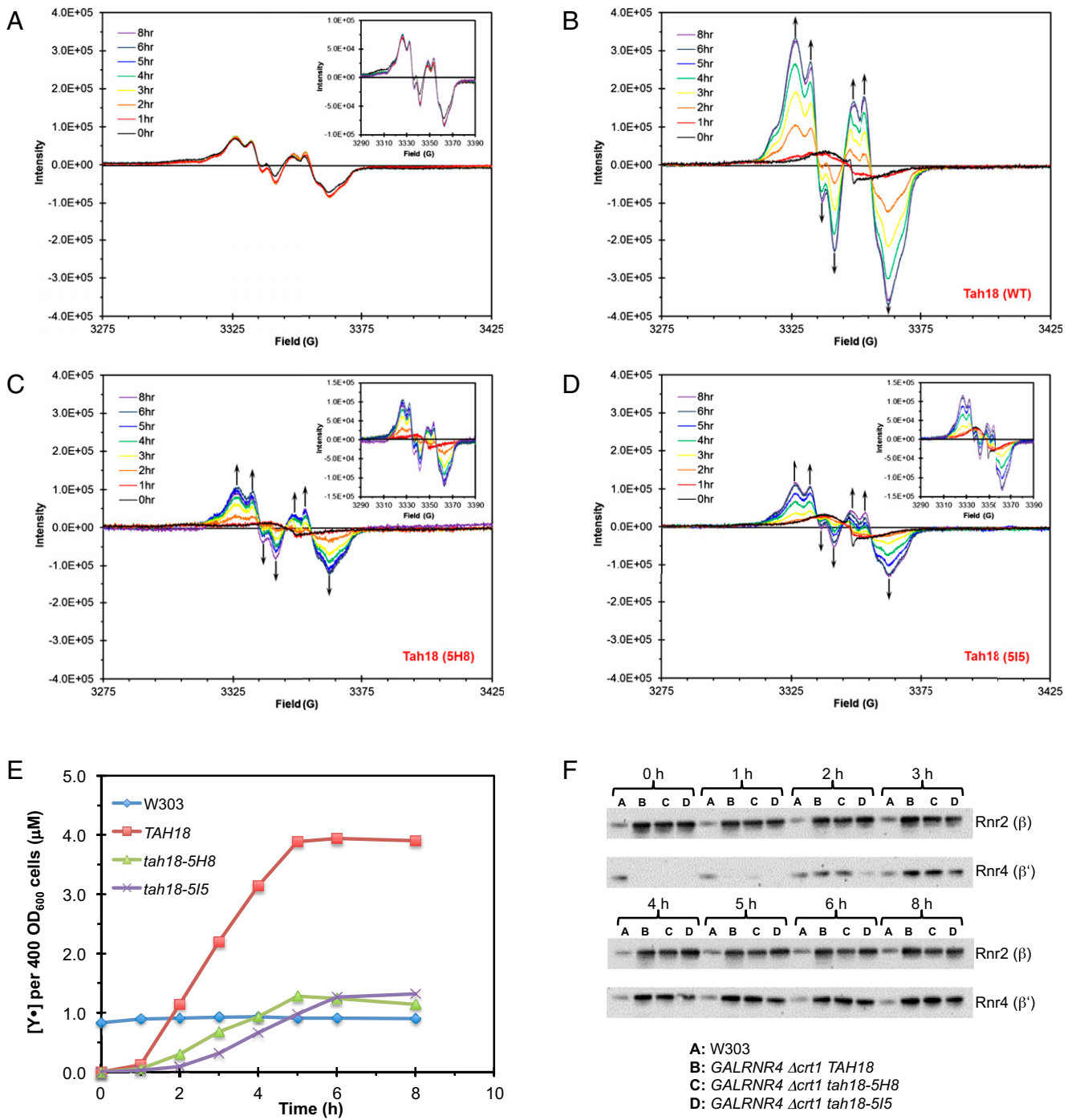
Fig. 7. Inactivation of Tah18 impairs reconstitution of ββ′ activity upon induction of β′ in *Δcrt1 GalRNR4* cells. (*A–D*) EPR spectra showing changes in Y• content at different time points after β′ induction in *TAH18* WT cells (*B*), in ts mutants *tah18-5H8* (*C*), and in *tah18-5I5* cells (*D*), all in the *GalRNR4 Δcrt1* background. EPR spectra of a WT W303 strain (*A*) are shown as controls. (*E*) Comparison of changes in Y• content over an 8-h time course of β′ induction. Signals of Y• were normalized against cell number (OD$_{600}$) at different time points. The Y• level remained unchanged in W303, which has *RNR4* under its endogenous promoter. (*F*) Comparison of Rnr2 (β) and Rnr4 (β′) protein levels during the time course of β′ induction. Western blots show constitutive and comparable Rnr2 (β) levels and induction of Rnr4 (β′) at different time points in *TAH18*, *tah18-5H8*, and *tah18-5I5* cells, all in the *GalRNR4Δcrt1* background.

sembly process (50). Because mitochondrial ISC is not affected by Dre2 deficiency (51), it was unclear how Aft1/Aft2 became activated in Dre2-depleted cells. One possible explanation is based on our model that Dre2–Tah18 supplies electrons to Grx3/Grx4 for their function in the delivery of iron for the assembly of all iron-requiring cofactors, including those in the mitochondria (Fig. 1*B*). This notion is supported by synthetic lethality between *grx3/4* and

dre2 mutants (13) and by interactions between Dre2 and Grx3 in both yeast and human (52, 53). Moreover, we show that the *CTH2* transcript is induced to a much greater extent in the *grx3/4* mutant than in *GalDRE2* mutant (Fig. 3*A*). Thus, it is possible that Dre2 depletion may cause deficiency in Grx3/4 activity, which could be sensed directly or indirectly by Aft1/Aft2, leading to transcriptional induction of *CTH2*. We noted that, unlike *CTH2,* another

member of the iron regulon *FET3* is induced in the *grx3/4* but not much in *GalDRE2* mutant, perhaps reflecting a differential degree of activation of Aft1/Aft2 in these mutants.

Second, we found that Dre2-depleted cells have an activated DNA-damage checkpoint resulting in transcriptional induction of *RNR3* as well as *RNR2/RNR4* through phosphorylation-mediated removal of repressor Crt1 from its target promoters. Thus, the apparent static level of ββ′ would result from the opposing effects of checkpoint-mediated transcriptional induction and Cth1/Cth2-mediated mRNA turnover of *RNR2/RNR4*. Consistent with this notion, Dre2-depleted cells have higher Rnr3 levels but lower ββ′ levels than WT cells. Cth1/Cth2 promote mRNA turnover not only of *RNR2/RNR4* but also of *WTM1*, which acts to prevent nuclear release of ββ′ and its colocalization with α (21, 22). The apparent paradoxical down-regulation of both ββ′ and its negative regulator Wtm1 suggests that, in an effort to optimize the use of limited iron, yeast cells prioritize nucleus-to-cytoplasm redistribution and iron loading of existing ββ′ proteins over the synthesis of more apo proteins.

Third, the findings in *GalDRE2* and *Δaft1* mutants of *RNR3* induction and Dif1 phosphorylation, two downstream events mediated by checkpoint kinase Dun1, indicate that the Mec1–Rad53–Dun1 checkpoint cascade can be activated in mutants defective in Fe-S cluster synthesis or cellular iron homeostasis. Fe-S cluster–binding domains have been found in an increasing number of nuclear proteins involved in DNA replication and repair including DNA primase, DNA helicases, and DNA polymerases (54). The importance of Dre2–Tah18 in DNA replication also was supported by the synthetic lethality between a ts mutant of *POL3* encoding the Fe-S cluster containing DNA polymerase δ and *dre2* and *tah18* mutant alleles (55). Our findings show that the Dre2–Tah18 complex is required for assembly of the di-iron enzyme RNR cluster and for cellular supplies of dNTP. As such, deficiencies in the CIA pathway or proper distribution of intracellular iron utilization would impact many aspects of DNA replication and repair directly, leading to checkpoint activation.

Our finding that removal of Cth1/Cth2 only partially restores the decrease of ββ′ levels in Dre2-depleted cells suggests additional, unidentified regulatory mechanism(s), likely instability of the apo-ββ′ proteins. Therefore, our focus was to identify strains with increased ββ′ levels so that cofactor Fe$^{III}_2$-Y• could be monitored in cells lacking Dre2 and Tah18. We achieved this goal by increasing intracellular manganese levels in the conditional strain *GalDRE2* via *Δpmr1* and by keeping β constitutively overexpressed in the *GalRNR4 tah18* ts mutant via *Δcrt1*. The results of our studies using these strategies strongly support the requirement of Dre2–Tah18 in RNR cluster assembly, either by delivering the obligatory reducing equivalent for RNR cluster formation in β (Eq. **1**) or by being involved indirectly in iron delivery. The finding of coimmunoprecipitation between Dre2 and Rnr2 (β) (Fig. 5*D*) is consistent with the proposed role of Dre2 in electron delivery. Because Dre2 also has been shown to interact with Grx3/Grx4, we further postulate that Dre2–Tah18 might provide the reducing equivalents to allow Fe^{2+} transfer from the [2Fe2S]-(GSH)$_2$ cluster at the Grx3/4 dimer interface to apo-ββ′.

The active cluster in both the di-iron– and Fe-S cluster–requiring proteins can form by self-assembly with varying degrees of efficiency in vitro (28, 56). Both require carefully controlled delivery of reducing equivalents. Thus, in both cases biosynthesis and perhaps maintenance pathways may have evolved to ensure highly efficient construction of an essential cofactor. The central role of Dre2–Tah18 in the assembly of the Fe-S cluster in many cytosolic and nuclear proteins, including enzymes involved in DNA replication and repair, complicated experimental designs to obtain evidence for our model (Fig. 1*B*). Our results together with previous studies by the Lill group (25) suggest that the CIA machinery and RNR cluster assembly share the same sources of iron, in the form of [2Fe2S]-(GSH)$_2$ from Grx3/Grx4, and also the same source of reducing equivalents from Dre2–Tah18. The point of bifurcation of the CIA and the RNR cluster assembly processes remains to be unraveled.

The pathway for Fe$^{III}_2$-Y• assembly is likely conserved between *S. cerevisiae* and human despite the differences in structures of the two β$_2$ subunits (heterodimer versus homodimer) (1). The mammalian Grx3, PICOT, recently has been shown to be required for multiple pathways in iron homeostasis, including biogenesis of the Fe-S cluster and hemoglobin maturation (31). The Dre2–Tah18 complex may function as the cytosolic equivalent of the mitochondrial Fd-Fre pair Yah1-Arh1 to deliver electrons to multiple and divergent pathways of iron cofactor biogenesis. The human counterparts of Dre2 and Tah18, CIAPIN1 and NDOR1, respectively, recently have been shown to function in their place in yeast cells in Fe-S cluster assembly in Leu1, a substrate of the CIA machinery (33, 51). It remains to be determined if CIAPIN1-NDOR1 are involved in the assembly of the Fe$^{III}_2$-Y• cluster of RNR and the Fe-S cluster of CIA in mammalian cells. Discovering the cellular machinery required for Fe$^{III}_2$-Y• assembly and repair would provide still another tier to the multilayered RNR regulation and would provide new insights into development of RNR-targeted therapeutics.

Experimental Procedures

Yeast Strains, Plasmids, and Growth Conditions. Yeast strains and plasmids used in this study are listed in Tables S1 and S2, respectively. Growth of yeast strains and genetic manipulations were as described (57). *GalDRE2* and *GalRNR4* strains were constructed by replacing sequences between nucleotides −50 and −1 of each endogenous promoter with the *GAL1* promoter (58). AXY1664, AXY1668, and AXY1696 were constructed by integrating an N-terminally Flag-tagged *TAH18* (WT) or *tah18-5H8* and *tah18-5I5* mutants into the *tah18::KanMX4* locus. Cell-cycle synchronization and FACS analysis were as described (59).

Protein Analysis. Yeast protein extracts were prepared by trichloroacetic acid precipitation (10) or alkaline treatment (60) for Western blotting and by lysis buffer B for immunoprecipitation (20). Antibodies used for immunoprecipitation and Western blotting were anti-Rnr2/3/4, as previously described (61), anti-G6PDH (Sigma-Aldrich), and monoclonal 9E10 (anti-Myc; Covance). Signals from protein blots were recorded and quantitated using ChemiDoc MP (Bio-Rad).

RNA Extraction, Reverse Transcription, and RT-qPCR. Total RNA was extracted from 2×10^8 cells by using a hot-phenol method (62). Total RNA (10 μg) was treated with 10 units of RNase-free DNase I (New England Biolabs) for 30 min at 37 °C to remove contaminating DNA. First-strand cDNA synthesis was carried out by M-MuLV reverse transcriptase (New England Biolabs) on aliquots of 1 μg RNA with a random primer mix. The single-stranded cDNA products were used in qPCR on a Bio-Rad CFX96 real-time PCR detection system based on SYBR Green fluorescence. Sequences of oligo pairs are listed in Table S3.

Whole-Cell EPR Spectroscopy and ββ′ Activity Assays in Permeabilized Cells. Whole-cell EPR spectroscopy, preparation of permeabilized yeast cells, and measurement of RNR activity were performed as described previously (13).

1. Nordlund P, Reichard P (2006) Ribonucleotide reductases. *Annu Rev Biochem* 75:681–706.
2. Stubbe J, van Der Donk WA (1998) Protein Radicals in Enzyme Catalysis. *Chem Rev* 98(2):705–762.
3. Hofer A, Crona M, Logan DT, Sjöberg BM (2012) DNA building blocks: Keeping control of manufacture. *Crit Rev Biochem Mol Biol* 47(1):50–63.
4. Rofougaran R, Vodnala M, Hofer A (2006) Enzymatically active mammalian ribonucleotide reductase exists primarily as an alpha6beta2 octamer. *J Biol Chem* 281(38):27705–27711.

5. Wang J, Lohman GJ, Stubbe J (2007) Enhanced subunit interactions with gemcitabine-5′-diphosphate inhibit ribonucleotide reductases. *Proc Natl Acad Sci USA* 104(36):14324–14329.

6. Fairman JW, et al. (2011) Structural basis for allosteric regulation of human ribonucleotide reductase by nucleotide-induced oligomerization. *Nat Struct Mol Biol* 18(3):316–322.

7. Kashlan OB, Cooperman BS (2003) Comprehensive model for allosteric regulation of mammalian ribonucleotide reductase: Refinements and consequences. *Biochemistry* 42(6):1696–1706.

8. Minnihan EC, Nocera DG, Stubbe J (2013) Reversible, long-range radical transfer in E. coli class la ribonucleotide reductase. *Acc Chem Res* 46(11):2524–2535.

9. Stubbe J, Nocera DG, Yee CS, Chang MC (2003) Radical initiation in the class I ribonucleotide reductase: Long-range proton-coupled electron transfer? *Chem Rev* 103(6):2167–2201.

10. An X, Zhang Z, Yang K, Huang M (2006) Cotransport of the heterodimeric small subunit of the Saccharomyces cerevisiae ribonucleotide reductase between the nucleus and the cytoplasm. *Genetics* 173(1):63–73.

11. Perlstein DL, et al. (2005) The active form of the Saccharomyces cerevisiae ribonucleotide reductase small subunit is a heterodimer in vitro and in vivo. *Biochemistry* 44(46):15366–15377.

12. Voegtli WC, Ge J, Perlstein DL, Stubbe J, Rosenzweig AC (2001) Structure of the yeast ribonucleotide reductase Y2Y4 heterodimer. *Proc Natl Acad Sci USA* 98(18):10073–10078.

13. Zhang Y, et al. (2011) Investigation of in vivo diferric tyrosyl radical formation in Saccharomyces cerevisiae Rnr2 protein: Requirement of Rnr4 and contribution of Grx3/4 AND Dre2 proteins. *J Biol Chem* 286(48):41499–41509.

14. Ortigosa AD, et al. (2006) Determination of the in vivo stoichiometry of tyrosyl radical per betabeta′ in Saccharomyces cerevisiae ribonucleotide reductase. *Biochemistry* 45(40):12282–12294.

15. Yao R, et al. (2003) Subcellular localization of yeast ribonucleotide reductase regulated by the DNA replication and damage checkpoint pathways. *Proc Natl Acad Sci USA* 100(11):6628–6633.

16. Huang MX, Zhou Z, Elledge SJ (1998) The DNA replication and damage checkpoint pathways induce transcription by inhibition of the Crt1 repressor. *Cell* 94(5):595–605.

17. Zhao X, Chabes A, Domkin V, Thelander L, Rothstein R (2001) The ribonucleotide reductase inhibitor Sml1 is a new target of the Mec1/Rad53 kinase cascade during growth and in response to DNA damage. *EMBO J* 20(13):3544–3553.

18. Zhao X, Muller EG, Rothstein R (1998) A suppressor of two essential checkpoint genes identifies a novel protein that negatively affects dNTP pools. *Mol Cell* 2(3):329–340.

19. Lee YD, Wang J, Stubbe J, Elledge SJ (2008) Dif1 is a DNA-damage-regulated facilitator of nuclear import for ribonucleotide reductase. *Mol Cell* 32(1):70–80.

20. Wu X, Huang M (2008) Dif1 controls subcellular localization of ribonucleotide reductase by mediating nuclear import of the R2 subunit. *Mol Cell Biol* 28(23):7156–7167.

21. Lee YD, Elledge SJ (2006) Control of ribonucleotide reductase localization through an anchoring mechanism involving Wtm1. *Genes Dev* 20(3):334–344.

22. Zhang Z, et al. (2006) Nuclear localization of the Saccharomyces cerevisiae ribonucleotide reductase small subunit requires a karyopherin and a WD40 repeat protein. *Proc Natl Acad Sci USA* 103(5):1422–1427.

23. Sanvisens N, Baño MC, Huang M, Puig S (2011) Regulation of ribonucleotide reductase in response to iron deficiency. *Mol Cell* 44(5):759–769.

24. Kaplan CD, Kaplan J (2009) Iron acquisition and transcriptional regulation. *Chem Rev* 109(10):4536–4552.

25. Mühlenhoff U, et al. (2010) Cytosolic monothiol glutaredoxins function in intracellular iron sensing and trafficking via their bound iron-sulfur cluster. *Cell Metab* 12(4):373–385.

26. Bollinger JM, Jr., et al. (1991) Mechanism of assembly of the tyrosyl radical-dinuclear iron cluster cofactor of ribonucleotide reductase. *Science* 253(5017):292–298.

27. Atkin CL, Thelander L, Reichard P, Lang G (1973) Iron and free radical in ribonucleotide reductase. Exchange of iron and Mössbauer spectroscopy of the protein B2 subunit of the Escherichia coli enzyme. *J Biol Chem* 248(21):7464–7472.

28. Cotruvo JA, Stubbe J (2011) Class I ribonucleotide reductases: Metallocofactor assembly and repair in vitro and in vivo. *Annu Rev Biochem* 80:733–767.

29. Yu Y, Wong J, Lovejoy DB, Kalinowski DS, Richardson DR (2006) Chelators at the cancer coalface: Desferrioxamine to Triapine and beyond. *Clin Cancer Res* 12(23):6876–6883.

30. Aye Y, Long MJ, Stubbe J (2012) Mechanistic studies of semicarbazone triapine targeting human ribonucleotide reductase in vitro and in mammalian cells: Tyrosyl radical quenching not involving reactive oxygen species. *J Biol Chem* 287(42):35768–35778.

31. Haunhorst P, et al. (2013) Crucial function of vertebrate glutaredoxin 3 (PICOT) in iron homeostasis and hemoglobin maturation. *Mol Biol Cell* 24(12):1895–1903.

32. Li H, Mapolelo DT, Randeniya S, Johnson MK, Outten CE (2012) Human glutaredoxin 3 forms [2Fe-2S]-bridged complexes with human BolA2. *Biochemistry* 51(8):1687–1696.

33. Netz DJ, et al. (2010) Tah18 transfers electrons to Dre2 in cytosolic iron-sulfur protein biogenesis. *Nat Chem Biol* 6(10):758–765.

34. Vernis L, et al. (2009) A newly identified essential complex, Dre2-Tah18, controls mitochondria integrity and cell death after oxidative stress in yeast. *PLoS ONE* 4(2):e4376.

35. Wu C-H, Jiang W, Krebs C, Stubbe J (2007) YfaE, a ferredoxin involved in diferric-tyrosyl radical maintenance in Escherichia coli ribonucleotide reductase. *Biochemistry* 46(41):11577–11588.

36. Lange H, Kaut A, Kispal G, Lill R (2000) A mitochondrial ferredoxin is essential for biogenesis of cellular iron-sulfur proteins. *Proc Natl Acad Sci USA* 97(3):1050–1055.

37. Li J, Saxena S, Pain D, Dancis A (2001) Adrenodoxin reductase homolog (Arh1p) of yeast mitochondria required for iron homeostasis. *J Biol Chem* 276(2):1503–1509.

38. Puig S, Askeland E, Thiele DJ (2005) Coordinated remodeling of cellular metabolism during iron deficiency through targeted mRNA degradation. *Cell* 120(1):99–110.

39. Martínez-Pastor M, Vergara SV, Puig S, Thiele DJ (2013) Negative feedback regulation of the yeast CTH1 and CTH2 mRNA binding proteins is required for adaptation to iron deficiency and iron supplementation. *Mol Cell Biol* 33(11):2178–2187.

40. Puig S, Vergara SV, Thiele DJ (2008) Cooperation of two mRNA-binding proteins drives metabolic adaptation to iron deficiency. *Cell Metab* 7(6):555–564.

41. Ojeda L, et al. (2006) Role of glutaredoxin-3 and glutaredoxin-4 in the iron regulation of the Aft1 transcriptional activator in Saccharomyces cerevisiae. *J Biol Chem* 281(26):17661–17669.

42. Courel M, Lallet S, Camadro JM, Blaiseau PL (2005) Direct activation of genes involved in intracellular iron use by the yeast iron-responsive transcription factor Aft2 without its paralog Aft1. *Mol Cell Biol* 25(15):6760–6771.

43. Tkach JM, et al. (2012) Dissecting DNA damage response pathways by analysing protein localization and abundance changes during DNA replication stress. *Nat Cell Biol* 14(9):966–976.

44. Elledge SJ, Davis RW (1990) Two genes differentially regulated in the cell cycle and by DNA-damaging agents encode alternative regulatory subunits of ribonucleotide reductase. *Genes Dev* 4(5):740–751.

45. Atta M, Nordlund P, Aberg A, Eklund H, Fontecave M (1992) Substitution of manganese for iron in ribonucleotide reductase from Escherichia coli. Spectroscopic and crystallographic characterization. *J Biol Chem* 267(29):20682–20688.

46. Culotta VC, Yang M, Hall MD (2005) Manganese transport and trafficking: Lessons learned from Saccharomyces cerevisiae. *Eukaryot Cell* 4(7):1159–1165.

47. McNaughton RL, et al. (2010) Probing in vivo Mn2+ speciation and oxidative stress resistance in yeast cells with electron-nuclear double resonance spectroscopy. *Proc Natl Acad Sci USA* 107(35):15335–15339.

48. Reddi AR, Culotta VC (2011) Regulation of manganese antioxidants by nutrient sensing pathways in Saccharomyces cerevisiae. *Genetics* 189(4):1261–1270.

49. Liu XF, Culotta VC (1994) The requirement for yeast superoxide dismutase is bypassed through mutations in BSD2, a novel metal homeostasis gene. *Mol Cell Biol* 14(11):7037–7045.

50. Chen OS, Hemenway S, Kaplan J (2002) Inhibition of Fe-S cluster biosynthesis decreases mitochondrial iron export: Evidence that Yfh1p affects Fe-S cluster synthesis. *Proc Natl Acad Sci USA* 99(19):12321–12326.

51. Zhang Y, et al. (2008) Dre2, a conserved eukaryotic Fe/S cluster protein, functions in cytosolic Fe/S protein biogenesis. *Mol Cell Biol* 28(18):5569–5582.

52. Saito Y, et al. (2011) PICOT is a molecule which binds to anamorsin. *Biochem Biophys Res Commun* 408(2):329–333.

53. Tarassov K, et al. (2008) An in vivo map of the yeast protein interactome. *Science* 320(5882):1465–1470.

54. White MF, Dillingham MS (2012) Iron-sulphur clusters in nucleic acid processing enzymes. *Curr Opin Struct Biol* 22(1):94–100.

55. Chanet R, Heude M (2003) Characterization of mutations that are synthetic lethal with pol3-13, a mutated allele of DNA polymerase delta in Saccharomyces cerevisiae. *Curr Genet* 43(5):337–350.

56. Malkin R, Rabinowitz JC (1966) The reconstitution of clostridial ferredoxin. *Biochem Biophys Res Commun* 23(6):822–827.

57. Burke D, Sawson D, Stearns T (2000) *Methods in Yeast Genetics: A Cold Spring Harbor Laboratory Course Manual* (Cold Spring Harbor Lab Press, Cold Spring Harbor, NY).

58. Longtine MS, et al. (1998) Additional modules for versatile and economical PCR-based gene deletion and modification in Saccharomyces cerevisiae. *Yeast* 14(10):953–961.

59. Gasch AP, et al. (2001) Genomic expression responses to DNA-damaging agents and the regulatory role of the yeast ATR homolog Mec1p. *Mol Biol Cell* 12(10):2987–3003.

60. Kushnirov VV (2000) Rapid and reliable protein extraction from yeast. *Yeast* 16(9):857–860.

61. Nguyen HH, Ge J, Perlstein DL, Stubbe J (1999) Purification of ribonucleotide reductase subunits Y1, Y2, Y3, and Y4 from yeast: Y4 plays a key role in diiron cluster assembly. *Proc Natl Acad Sci USA* 96(22):12339–12344.

62. Köhrer K, Domdey H (1991) Preparation of high molecular weight RNA. *Methods Enzymol* 194:398–405.